Nonadiabatic tunneling in circularly polarized laser fields: Physical picture and calculations

Ingo Barth and Olga Smirnova
Max Born Institute, Max-Born-Strasse 2A, D-12489 Berlin, Germany
(Received 2 August 2011; published 16 December 2011)

We consider selectivity of strong-field ionization in circularly polarized laser fields to the sense of electron rotation in the laser polarization plane in the initial state. We show that, in contrast to the textbook examples of one-photon ionization and bound-state excitations with increase in the electron angular momentum, and also in contrast to the well-studied ionization of Rydberg atoms in microwave fields, which all prefer corotating electrons, optical tunneling selectively depletes states where the electron initially rotates against the laser field. We also show that key assumptions regarding adiabaticity of optical tunneling may quickly become inaccurate in typical experimental conditions.

DOI: 10.1103/PhysRevA.84.063415 PACS number(s): 42.50.Hz, 32.80.Rm, 33.80.Wz

I. INTRODUCTION

Electron tunneling from atoms and molecules in strong laser fields is usually described as an adiabatic process. It implies that the motion of the tunneling barrier does not affect the electron dynamics during tunneling. In circularly polarized fields, the adiabatic picture assumes that the electron escapes along the instantaneous direction of the electric field, ignoring its rotation in each tunneling event. If this is not the case, would tunneling deplete different m states selectively? Specifically, would electrons corotating with the barrier ($m > 0$) tunnel easier than the electrons rotating in the opposite direction ($m < 0$)? Surprisingly, this question has not been addressed, in spite of a large body of experimental work performed with circularly polarized fields applied to initial states with $m \neq 0$ in nonadiabatic tunneling regime [1–5]. Here we answer this question by deriving virtually exact analytical solutions for short-range potentials. Including effects of the long-range Coulomb potential in a standard way does not change our conclusions. Our results have implications for understanding and interpreting "attosecond angular streaking" experiments [1–5], where a strong circularly polarized field is used as a probe of electron dynamics in atoms and molecules. Currently, interpretation of these experiments relies on the adiabatic picture of ionization, which as we show quickly becomes inaccurate for typical experimental conditions.

In the case of one-photon ionization the preference for the sign of m is well known. For transitions which increase the angular momentum of the electron, the bound m state corotating with the circular field ($m > 0$) will be depleted more efficiently than the m state in which the electron rotates in the opposite direction [6]. The same is true for the ionization of circular Rydberg states (and of rotating Rydberg wave packets) in circularly polarized microwave fields. Ionization is much more likely for the Rydberg electron corotating with the field, preferably with the same angular velocity [7,8]. It proceeds via successive excitations of the manifold of Rydberg states, which is more efficient for corotating electrons. Would the same preference appear in tunneling, where real excitations are not involved?

Formally, tunneling corresponds to the nonresonant absorption of many photons $N \gg 1$. For a right-polarized circular field, each absorbed photon increases the magnetic quantum number by $\Delta m = +1$. Which of the degenerate m sublevels of the initial state p has better chances to be depleted: $m = 1$, $m = -1$, or $m = 0$? In other words, which final state is more likely to be created: $m_f = N + 1$, $m_f = N - 1$, or $m_f = N$? We show that, in contrast to one-photon ionization and ionization from Rydberg states in microwave fields [7,8], in tunneling the counterrotating electron has significantly better chances to penetrate the barrier than corotating electron (about three times higher for typical experimental conditions), while $m = 0$ is suppressed by orders of magnitude. Even though the difference in the final m_f is minimal, the sensitivity to initial m is high. Thus, the use of the adiabatic assumption and the quasistatic tunneling rates are inaccurate in typical experimental conditions. It is also commonly assumed that the electron after tunneling has zero average velocity perpendicular to the field. Our analysis shows that this assumption also becomes inaccurate in typical cases.

II. PHYSICAL PICTURE

Let us first try to understand this result using qualitative arguments. Consider strong-field ionization in right (+) or left (−) circularly polarized laser fields:

$$\mathbf{E}_{\pm}(t) = \mathcal{E}[\cos(\omega t)\,\mathbf{e}_x \pm \sin(\omega t)\,\mathbf{e}_y]. \tag{1}$$

The axes are shown in Fig. 1. Strong-field ionization is successfully described using semiclassical approaches, due to large action associated with the electron motion in the strong laser field. For each final momentum of the electron registered at the detector, the least action principle specifies a particular trajectory for the electron tunneling. However, since the electron moves in the classically forbidden (underbarrier) region, this trajectory evolves in complex time. The dominant, exponential part of the tunneling rate $w_{\mathbf{k}}(\mathcal{E},\omega)$ is characterized by the electron action accumulated "under the barrier" along this trajectory:

$$w_{\mathbf{k}}(\mathcal{E},\omega) \propto e^{-2\mathrm{Im}\,S(\mathbf{k},t_i)},$$
$$S(\mathbf{k},t_i) = -1/2\int_{t_i}^{\mathrm{Re}\,t_i} [\mathbf{k} + \mathbf{A}_{\pm}(t)]^2 dt + I_p t_i, \tag{2}$$

where $\mathbf{A}_{\pm}(t)$ is defined as

$$\mathbf{E}_{\pm}(t) = -\frac{d}{dt}\mathbf{A}_{\pm}(t),$$
$$\mathbf{A}_{\pm}(t) = -A_0[\sin(\omega t)\,\mathbf{e}_x \mp \cos(\omega t)\,\mathbf{e}_y], \tag{3}$$

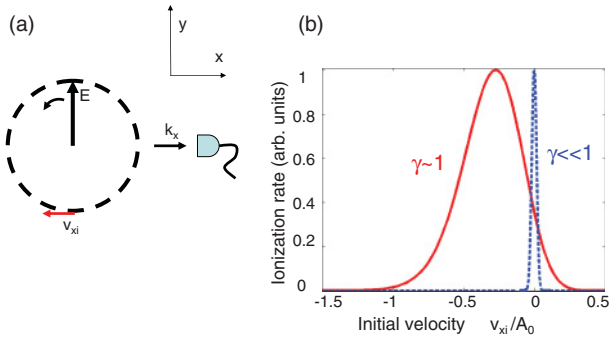

FIG. 1. (Color online) Kinematics of electron tunneling through rotating barrier. (a) Right circularly polarized laser field $\mathbf{E}_+$ creates the tunneling barrier rotating counterclockwise. The electron observed at the detector placed along the x axis exits the barrier along the y axis, opposite to the direction of the laser field $\mathbf{E}_+$, i.e. in the negative direction of y axis. (b) Ionization rate estimated with exponential accuracy [Eq. (5)] for $\gamma \sim 1$ (solid red line) is maximal for the initial velocity $v_{xi} < 0$ and it corresponds to electron rotating clockwise. In the adiabatic limit ($\gamma \ll 1$) the distribution of initial transversal velocities becomes symmetric and is centered around zero (dashed blue line).

$\mathbf{k}$ is the final momentum observed at the detector, I_p is the ionization potential, $A_0 = \frac{\mathcal{E}}{\omega}$ is velocity amplitude of electron oscillations in the laser field, and $t_i = \mathrm{Re}\, t_i + i\,\mathrm{Im}\, t_i$ is the so-called (complex) time of ionization, which is uniquely linked to $\mathbf{k}$.

Complex time t_i can be interpreted as the time of entering into the barrier, while its real part $\mathrm{Re}\, t_i$ is the time of exiting the barrier [9]. For continuous-wave circularly polarized field and final momenta $k_x = k\cos\theta$, $k_y = k\sin\theta$ in the polarization plane, and $k_z = 0$, these times are [10,11]

$$\begin{aligned} \omega \mathrm{Re}\, t_i &= \frac{\pi}{2} + 2\pi N \pm \theta \qquad (N \in \mathbb{Z}), \\ \omega\, \mathrm{Im}\, t_i &= \operatorname{arcosh} \chi, \qquad \chi(k) = \frac{A_0}{2k}\left[\left(\frac{k}{A_0}\right)^2 + \gamma^2 + 1\right]. \end{aligned} \tag{4}$$

Here $\gamma = \sqrt{2I_p}/A_0$ is the Keldysh parameter [12] discriminating among adiabatic tunneling ($\gamma \ll 1$), nonadiabatic tunneling [13] ($\gamma \sim 1$), and multiphoton ionization ($\gamma \gg 1$). Substituting Eqs. (4) into Eqs. (2) obtains

$$w_{\mathbf{k}}(\mathcal{E},\omega) \propto e^{-\frac{2A_0 k}{\omega}(\chi \operatorname{arcosh}\chi - \sqrt{\chi^2-1})}. \tag{5}$$

The maximal ionization rate given by Eq. (5) corresponds to the final momentum $k_0 = A_0\sqrt{1+\gamma^2}\sqrt{\frac{1-\zeta_0}{1+\zeta_0}}$ for any angle θ. The parameter $0 \leqslant \zeta_0 \leqslant 1$ satisfies the equation $\sqrt{\frac{\zeta_0^2+\gamma^2}{1+\gamma^2}} = \tanh\frac{1}{1-\zeta_0}\sqrt{\frac{\zeta_0^2+\gamma^2}{1+\gamma^2}}$. Note that $\zeta_0 \simeq \gamma^2/3$ for $\gamma \ll 1$, and $\zeta_0 \simeq 1 - 1/\ln\gamma$ for $\gamma \gg 1$ [10]. For each observation angle θ, the momentum k_0 defines the "optimal" trajectory, which corresponds to the highest ionization rate. Consider right circular polarization. Let us follow one of these optimal trajectories, which corresponds to the the electron observed at the detector along the x axis [$\theta = 0$; see Fig. 1(a)]. Equation (4) tells us that this electron has been ejected at $\omega \mathrm{Re}\, t_i = \pi/2$, when the direction of the instantaneous electric field is parallel to the y axis and electron velocity along the y axis $v_y = 0$. When the electron enters the barrier at complex time t_i, v_y is purely imaginary: $v_{yi} = -iA_0\sqrt{\chi(k_0)^2 - 1}$, just as one would expect for tunneling in the field pointing along the y axis. The transverse velocity at this time is $v_{xi} = [k_0 - A_0\chi(k_0)]$. In the adiabatic limit ($\gamma \ll 1$) $v_{xi} \simeq -\sqrt{2I_p}\gamma/3$, the distribution of initial transversal velocities becomes symmetric and is centered around zero ($v_{xi} \simeq 0$) [see Fig. 1(b), blue curve], also as usually expected in the direction perpendicular to the field. However, in the regime of nonadiabatic tunneling ($\gamma \sim 1$) [13], the transverse initial velocity distribution is asymmetric; its peak $v_{xi} = -A_0\sqrt{1+\gamma^2}\zeta_0/\sqrt{1-\zeta_0^2} < 0$ is substantially offset from zero [see Fig. 1(b), red curve] and corresponds to negative velocities [14]. The electrons which rotate opposite to the direction of the laser field are more likely to have this velocity than those corotating with the field. Therefore, the p_- orbital will be more strongly depleted than the p_+ orbital. The hole created after ionization will rotate opposite to the direction of the laser field.

To complete the analysis, one has to take into account the pre-exponential terms in the ionization rate $w_{\mathbf{k}}(\mathcal{E},\omega)$ which depend on the particular shape of the initial state, that is, the presence of the required momentum components in the initial wave function. We have derived simple analytical expressions which quantitatively describe this effect (see Fig. 2; the derivation is discussed below) for right circularly polarized field (left polarization is treated similarly [15]):

$$w_{p_m}(\mathcal{E},\omega) = I_p|C_{\kappa l}|^2\frac{\mathcal{E}}{2\mathcal{E}_0}h_{p_m}(\gamma)\, e^{-\frac{2\mathcal{E}_0}{3\mathcal{E}}g(\gamma)}, \quad m = \pm 1, \tag{6}$$

where $\mathcal{E}_0 = (2I_p)^{3/2}$, $\kappa = \sqrt{2I_p}$, $C_{\kappa l}$ characterizes the asymptotic behavior of the radial wave function with the orbital quantum number l. Results for p_0 orbital will be exposed in our companion paper [11]. The function $g(\gamma)$ in the exponent is the same as in the case of s orbitals:

$$g(\gamma) = \frac{3\zeta_0}{\gamma^2(1-\zeta_0^2)}\sqrt{(1+\gamma^2)\left(\zeta_0^2/\gamma^2 + 1\right)}, \tag{7}$$

and the factors $h_{p_m}(\gamma)$ for $p_\pm$ states

$$h_{p_m}(\gamma) = h_s(\gamma)\frac{3(1+\gamma^2)}{2(1-\zeta_0^2)}\left(\sqrt{\frac{\zeta_0^2/\gamma^2+1}{1+\gamma^2}} \mp \frac{\zeta_0}{\gamma}\,\mathrm{sgn}(m)\right)^2 \tag{8}$$

are expressed via the factor $h_s(\gamma)$ for the s state:

$$h_s(\gamma) = (1-\zeta_0)\sqrt{\frac{(1+\gamma^2)(1-\zeta_0^2)}{(\zeta_0^2/\gamma^2+1)(2\zeta_0^2/\gamma^2+\zeta_0^2+1)}}. \tag{9}$$

The result for the s state has been previously derived in [10]. The limiting cases of tunnel and multiphoton ionization in right circularly polarized field [15] yield

$$\begin{aligned} \left.\frac{w_{p_-}}{w_{p_+}}\right|_{\gamma\ll 1} &= 1 + \frac{4\gamma}{3} > 1, \\ \left.\frac{w_{p_-}}{w_{p_+}}\right|_{\gamma\gg 1} &= (2\ln\gamma)^2 \gg 1. \end{aligned} \tag{10}$$

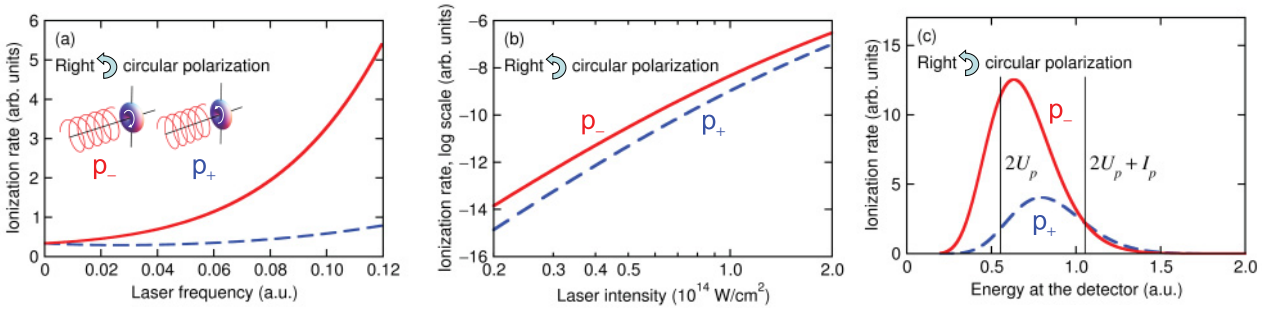

FIG. 2. (Color online) Ionization rate [Eqs. (6)–(9)] for $p_\pm$ orbitals and right circular polarization. (a) Ionization rate vs laser frequency for Kr ground $4p$ state ($I_p = 0.5$ a.u.) and laser field $\mathcal{E} = 0.06$ a.u. (b) Ionization rate vs laser intensity for Kr ground $4p$ state ($I_p = 0.5$ a.u.) and laser frequency $\omega = 0.057$ a.u. (c) Photoelectron energy distribution at the detector [Eq. (19)] for p_- (solid red line) and p_+ (dashed blue line) orbitals, for Kr ground $4p$ state ($I_p = 0.5$ a.u.), laser frequency $\omega = 0.057$ a.u., $\mathcal{E} = 0.06$ a.u. Electrons with energy $E^o_{\rm kin} = 2U_p + I_p$ (vertical line) correlate to nonrotating hole, low-energy electrons $E < E^o_{\rm kin}$ correlate to counterrotating holes, and higher energy electrons $E > E^o_{\rm kin}$ correlate to corotating holes. In the adiabatic case ($\gamma = 0$) photoelectron distributions are peaked at $2U_p$ and are the same for p_+ and p_- orbitals.

Equations (6)–(9) and are based on the Perelomov, Popov and Teren'tev (PPT) [10] approach. As is known [16], this approach is virtually exact for short-range potentials. Deviations from the exact solution are due to the following two approximations: (i) the Stark shift of the initial state is not included, and (ii) the saddle point method is used. Comparison with the exact solution for a δ potential [16] shows that the errors introduced by the saddle point method are small for low frequencies $\omega \ll I_p$ and field strengths $\mathcal{E} \ll (2I_p)^{3/2}$. While the results [Eqs. (6)–(9)] are general, the Stark shifts are system specific and can be calculated separately on a case-by-case basis [5,17] and incorporated into Eqs. (6)–(9). The Coulomb corrections can be introduced using standard recipes [9,18] involving the time integration of the Coulomb potential along the optimal trajectory. Since this trajectory is the same for p_+ and p_- states, the Coulomb correction in its standard form will equally affect the ionization rates from all p orbitals. Thus, it will not change our results for the ratio w_{p_-}/w_{p_+}. In contrast to the PPT theory, the velocity gauge strong-field approximation (SFA) [19] provides only exponential accuracy even for the short-range potentials and cannot provide the correct answer in our case, since all the effect is in the prefactor of the ionization rate. In fact, Ref. [20] has failed to find the difference in strong-field ionization from the p_+ and p_- orbitals by circular fields. The deficiencies of the velocity gauge SFA even for short-range potential have now been clearly documented using comparison with the exact analytical treatment [21] and with full numerical simulations [22–24].

III. CALCULATIONS

We now derive Eqs. (6)–(9). Following the PPT approach [10], we obtain [11] the total ionization rate as a sum over multiphoton channels:

$$w(\mathcal{E},\omega) = 2\pi \sum_{n\geqslant n_0}^{\infty} \int d\mathbf{k}\, \delta\left(\frac{k^2}{2} - \frac{k_n^2}{2}\right) |F_n(\mathbf{k},\omega)|^2 , \qquad (11)$$

where the final kinetic energy of the electron $E_{\rm kin} = \frac{k_n^2}{2}$ is

$$\frac{k_n^2}{2} = (n - n_0)\omega, \quad n_0 = \frac{I_p + 2U_p}{\omega}, \quad U_p = \frac{\mathcal{E}^2}{4\omega^2}, \qquad (12)$$

and n_0 is the minimal number of photons required for ionization. The functions $|F_n(\mathbf{k},\omega)|^2$ describe the probability of each multiphoton process:

$$|F_n(\mathbf{k},\omega)|^2_{k=k_n} = \frac{\omega^2}{4\pi^2} \left| \int_{-\pi/\omega}^{\pi/\omega} dt\, \phi_{lm}(\mathbf{v}(t)) e^{iS(\mathbf{k},t)} \right|^2_{k=k_n} . \qquad (13)$$

The prefactor is proportional to the specific momentum component of the initial wave function $\varphi_{lm}(\mathbf{r})$, corresponding to the instantaneous electron velocity $\mathbf{v}(t) = \mathbf{k} + \mathbf{A}_\pm(t)$:

$$\phi_{lm}(\mathbf{v}(t)) = \frac{1}{2}(\mathbf{v}(t)^2 + 2I_p)\tilde{\varphi}_{lm}(\mathbf{v}(t)),$$
$$\tilde{\varphi}_{lm}(\mathbf{k}) = \frac{1}{(2\pi)^{3/2}} \int d\mathbf{r}\, e^{-i\mathbf{kr}} \varphi_{lm}(\mathbf{r}). \qquad (14)$$

The saddle point method selects complex ionization time t_i [Eq. (4)] and yields a simple expression for functions $|F_n(\mathbf{k},\omega)|^2$:

$$|F_n(\mathbf{k},\omega)|^2_{k=k_n} = \frac{\omega^2}{4\pi^2} \left| \phi_{lm}(\mathbf{v}(t_i))\, e^{iS(\mathbf{k},t_i)} \sqrt{\frac{2\pi}{S''(\mathbf{k},t_i)}} \right|^2_{k=k_n} . \qquad (15)$$

The ionization time is the solution of the saddle point equation: $\partial S/\partial t = \mathbf{v}(t_i)^2/2 + I_p = 0$. The saddle point method tells us that the integral in Eq. (13) is accumulated mostly in the small region around the ionization time t_i. The width of this region is determined by the second derivative of the action $1/\sqrt{S''(\mathbf{k},t_i)}$. The initial electron velocity $\mathbf{v}(t_i)$ specifies the required momentum component of the initial wave function. The amount of this momentum component is different for p_+ and p_- orbitals. The initial electron velocity $\mathbf{v}(t_i)$ coincides with the pole of the initial wave function in the momentum

representation. In coordinate representation, it corresponds to the wave function asymptotically far from the core:

$$\varphi_{lm}(r,\theta_r,\phi_r) = C_{\kappa l}\kappa^{3/2}\frac{e^{-\kappa r}}{\kappa r}Y_{lm}(\theta_r,\phi_r), \tag{16}$$

with the constant $C_{\kappa l}$, depending on $\kappa = \sqrt{2I_p}$ and l and details of the potential near the core. Transforming Eq. (16) to the momentum space, we obtain

$$|F_n(\mathbf{k},\omega)|^2_{k=k_n} = |C_{\kappa l}|^2\frac{\omega\gamma}{k_\rho}\frac{2l+1}{16\pi^3}\frac{(l-|m|)!}{(l+|m|)!}\left|P_l^{|m|}\left(\frac{ik_z}{\kappa}\right)\right|^2 \times |e^{im\phi_v}|^2\left.\frac{e^{-2\,\mathrm{Im}\,S(\mathbf{k},t_i)}}{\sqrt{\chi^2(k_\rho)+k_z^4/\left(4k_\rho^2A_0^2\right)-1}}\right|_{k=k_n}, \tag{17}$$

where ϕ_v is "tunneling angle," $\tan(\phi_v) = v_y(t_i)/v_x(t_i)$, and $k = \sqrt{k_\rho^2+k_z^2}$. The difference in ionization from p_+ and p_- states is solely due to the factor $|e^{im\phi_v}|^2$, which is not equal to unity, since the tunneling angle ϕ_v is complex. By evaluating $|e^{im\phi_v}|^2$ and other factors in Eq. (17) explicitly [25] and introducing a dimensionless parameter $\zeta = 2n_0/n - 1$ we obtain the final expression for ionization rate from $p_\pm$ orbitals in right [15] circularly polarized laser fields:

$$w_{p_m}(\mathcal{E},\omega) = \sum_{n\geqslant n_0}^{\infty} w_n^{p_m}(\mathcal{E},\omega), \tag{18}$$

where $w_n^{p_m}(\mathcal{E},\omega)$ describes electron energy distribution $[E_{\mathrm{kin}} = k_n^2/2 = (n-n_0)\omega]$:

$$w_n^{p_m}(\mathcal{E},\omega) = \frac{3|C_{\kappa 1}|^2 I_p}{8\sqrt{2\pi}\,n_0^{3/2}}\left(1+\frac{1}{\gamma^2}\right)^{3/2}\frac{1}{\sqrt{1-\zeta}}\left(\frac{1+\gamma^2}{\zeta^2+\gamma^2}\right)^{3/4} \times \left(\sqrt{\frac{\zeta^2+\gamma^2}{1+\gamma^2}} - \zeta\,\mathrm{sgn}(m)\right)^2 \times e^{-\frac{4n_0}{1+\zeta}\left(\mathrm{artanh}\sqrt{\frac{\zeta^2+\gamma^2}{1+\gamma^2}}-\sqrt{\frac{\zeta^2+\gamma^2}{1+\gamma^2}}\right)}. \tag{19}$$

To evaluate the total ionization rate, the summation over n can be replaced with integration over ζ; that is, $\sum_{n\geqslant n_0}^{\infty} \approx \int_{n_0}^{\infty} dn = 2n_0\int_{-1}^{1}\frac{d\zeta}{(1+\zeta)^2}$. The application of the saddle point method for $I_p \gg \omega$ (i.e., $n_0 \gg 1$) for integration over ζ yields the compact expressions for ionization rate from $p_\pm$ orbitals given above in Eqs. (6)–(9).

IV. CONCLUSIONS

Thus, counter to standard cases of one-photon ionization and excitation and multiphoton ionization of Rydberg states [26], tunneling in circularly polarized fields selects counterrotating orbitals.

Photoelectron spectra are also different for electrons coming from different orbitals [Fig. 2(c)]. There is a unique final kinetic energy $E^o_{\mathrm{kin}} = 2U_p + I_p$ for which the amount of electrons coming from p_+ and p_- orbitals is exactly the same. In terms of the setup presented in Fig. 1, it corresponds to the component of their momentum-space wave function with $v_{xi} = 0$. Obviously, there is "an equal amount of such electrons" in p_+ and p_- orbitals. The final kinetic energy of the electron uniquely indicates the strength and the direction of the ring current [28,29] generated in the ion, measured in correlation with the electron. Low-energy electrons $E_{\mathrm{kin}} < E^o_{\mathrm{kin}}$ correlate to the ions with positive ring current, while higher energy electrons $E_{\mathrm{kin}} > E^o_{\mathrm{kin}}$ correlate to the ions with negative ring currents. Since the signal from p_- orbital dominates, the ring current in the ion can be detected even if the electron energy has not been measured, for example, by using a setup similar to that in Ref. [30], where the hole dynamics upon strong-field ionization has been directly probed in real time.

Note that, contrary to standard assumptions [1–5], in nonadiabatic tunneling, optimal trajectories for both p_+ and p_- electrons have nonzero velocities in the observation direction just after exiting the barrier: $v_x = k_0 - A_0$. That is why the peaks of the kinetic energy distributions for both p_+ and p_- electrons are shifted beyond $2U_p$ [Fig. 2(c)]. For $\gamma \ll 1$ the shift disappears as expected [31] and all peaks tend toward the $2U_p$ value. However, for $\gamma \sim 1$ nonzero average transverse velocities of electron after tunneling are substantial and may be responsible for the enhanced probability of nonsequential double ionization in circularly polarized fields [32].

We are grateful to M. Ivanov for reading the manuscript and useful suggestions. We gratefully acknowledge stimulating discussions with M. Ivanov, U. Keller, E. Goulielmakis, J. Manz, and A. Wirth. The work was supported by the DFG Grant No. Sm 292/2-1 and a SAW grant of the Leibniz Society.

[1] P. Eckle *et al.*, Nat. Phys. **4**, 565 (2008).
[2] P. Eckle *et al.*, Science **322**, 1525 (2008).
[3] H. Akagi *et al.*, Science **325**, 1364 (2009).
[4] A. P. Pfeiffer *et al.*, Nat. Phys. **7**, 428 (2011).
[5] A. P. Pfeiffer *et al.*, Nat. Phys. (2011), doi: 10.1038/nphys2125.
[6] H. Bethe, *Intermediate Quantum Mechanics* (W. A. Benjamin, Inc., New York, 1964).
[7] K. Rzazewski and B. Piraux, Phys. Rev. A **47**, R1612 (1993).
[8] J. Zakrzewski, D. Delande, J. C. Gay, and K. Rzazewski, Phys. Rev. A **47**, R2468 (1993).
[9] A. M. Perelomov and V. S. Popov, Sov. Phys. JETP **25**, 336 (1967).
[10] A. M. Perelomov, V. S. Popov, and M. V. Terentev, Sov. Phys. JETP **23**, 924 (1966).
[11] I. Barth and O. Smirnova, Phys. Rev. A (to be published).
[12] L. V. Keldysh, Sov. Phys. JETP **20**, 1307 (1965).
[13] G. L. Yudin and M. Yu. Ivanov, Phys. Rev. A **64**, 013409 (2001).
[14] Changing the sense of rotation of the laser polarization does not change the electron velocity v_{xi}; it is determined by the position

of the detector. However, it changes to opposite the direction of the field during tunneling and hence changes to opposite the electron coordinate during tunneling. Thus, as expected, the favored angular momentum is reversed.

[15] Here and in the following for brevity we consider only the case of right circular polarization. The expressions for left circular polarization and p_+ (p_-) orbital are the same as for right circular polarization and p_- (p_+) orbital.

[16] N. L. Manakov and L. P. Rapoport, Sov. Phys. JETP **42**, 430 (1976).

[17] E. V. Koryukina, J. Phys. D **38**, 3296 (2005).

[18] S. V. Popruzhenko, V. D. Mur, V. S. Popov, and D. Bauer, Phys. Rev. Lett. **101**, 193003 (2008).

[19] H. R. Reiss, Phys. Rev. A **22**, 1786 (1980).

[20] J. H. Bauer, Phys. Rev. A **83**, 035402 (2011).

[21] M. V. Frolov, N. L. Manakov, E. A. Pronin, and A. F. Starace, Phys. Rev. Lett. **91**, 053003 (2003); J. Phys. B **36**, L419 (2003).

[22] D. Bauer, D. B. Milosevic, and W. Becker, Phys. Rev. A **72**, 023415 (2005).

[23] Y. V. Vanne and A. Saenz, Phys. Rev. A **82**, 011403(R) (2010).

[24] A. M. Popov, M. A. Tikhonov, O. V. Tikhonova, and E. A. Volkova, Laser Phys. **19**, 191 (2011).

[25] Transformation from Eq. (17) to Eq. (18) involves an additional approximation $k_z \ll \sqrt{k_x^2 + k_y^2}$ which is accurate for ($\gamma \leqslant 1$) and introduces the error of about 15% for p_- and p_+ orbitals for large γ [11].

[26] In contrast to tunneling, ionization of Rydberg states in microwave fields occurs via real excitations followed by over-the-barrier ionization. The preference for intial m changes because the ionization mechanisms are very different, even though in both cases (Rydberg states and ground state considered here) ionization requires many photons. In case of strong-field ionization from the ground state, one can neglect the excitation dynamics prior ionization, if all the excited states are well separated from the ground state. In all Keldysh-like theories (such as PPT), any real excitations before ionization are explicitly excluded (see, e.g., [27]), making tunneling the dominant ionization mechanism. The same assumption does not work for manifolds of Rydberg states, where the excitation dynamics prior to ionization is crucial.

[27] M. Ivanov *et al.*, J. Mod. Opt. **52**, 165 (2005).

[28] I. Barth and J. Manz, Phys. Rev. A **75**, 012510 (2007).

[29] I. Barth and J. Manz, in *Progress in Ultrafast Intense Laser Science VI*, edited by K. Yamanouchi, A. D. Bandrauk, and G. Gerber, Springer Series in Chemical Physics Vol. 99 (Springer, Berlin, 2010).

[30] E. Goulielmakis *et al.*, Nature (London) **466**, 739 (2010).

[31] P. B. Corkum, N. H. Burnett, and F. Brunel, Phys. Rev. Lett. **62**, 1259 (1989).

[32] Xu Wang and J. H. Eberly, Phys. Rev. Lett. **105**, 083001 (2010).